



Article

A Study on the Volume Expansion of Vanadium-Based Alloy Powders and Compacts During Hydrogen Sorption

Mojia Li ¹, Yunfeng Hu ², Hanyang Kong ¹, Qiuwei Huang ¹, Yusong Chen ¹ and Yigang Yan ^{1,*}

¹ Institute of New Energy and Low-Carbon Technology, Sichuan University, Chengdu 610207, China; limojia@stu.scu.edu.cn (M.L.); hanyang_kong@163.com (H.K.); huangqiuwei2022@163.com (Q.H.); ty505606@outlook.com (Y.C.)

² Key Laboratory of Advanced Technologies of Materials, Ministry of Education, School of Materials Science and Engineering, Southwest Jiaotong University, Chengdu 610031, China; huyfeng@my.swjtu.edu.cn

* Correspondence: yigang.yan@scu.edu.cn

Abstract: Storing hydrogen in solid metal hydrides provides a safe and efficient storage approach. However, the large volume expansion of metal hydrides during hydrogen absorption imposes substantial stresses on the wall of a hydrogen storage tank. In this study, volume expansion behavior of a V-based hydrogen storage alloy, $V_{61}Cr_{24}Ti_{12}Ce_3$, with body-centered-cubic, was investigated using a self-developed in situ expansion testing device. The lattice expansion of the $V_{61}Cr_{24}Ti_{12}Ce_3$ alloy after full hydrogenation was determined to be 37.85% using X-ray diffraction(XRD). The powder bed, composed of alloy powder with an average size of 3.35 mm in diameter, displays a large volume expansion ratio of 131% at the first hydrogen absorption cycle and 40–45% in the following four cycles. The stable compact bed, made of alloy powders, organic silicone gel, and graphite flakes, shows significantly smaller volume expansion ratio, which is 97% at the first cycle and 21% at the second cycle, and stabilizes at 13% in the following cycles. Also, the compact bed shows similar hydrogen absorption capacity, but faster absorption kinetics compared to the powder bed.

Keywords: V-Ti-Cr alloy; volume expansion; metal hydride compact; organic silicone gel; graphite



Citation: Li, M.; Hu, Y.; Kong, H.; Huang, Q.; Chen, Y.; Yan, Y. A Study on the Volume Expansion of Vanadium-Based Alloy Powders and Compacts During Hydrogen Sorption. *Inorganics* **2024**, *12*, 318. <https://doi.org/10.3390/inorganics12120318>

Academic Editor: Rainer Niewa

Received: 24 November 2024

Accepted: 29 November 2024

Published: 8 December 2024



Copyright: © 2024 by the authors. Licensee MDPI, Basel, Switzerland. This article is an open access article distributed under the terms and conditions of the Creative Commons Attribution (CC BY) license (<https://creativecommons.org/licenses/by/4.0/>).

1. Introduction

To achieve the sustainable development of our society, a stable supply of environmentally harmless clean energy is essential. Renewable energies like solar and wind have great potential, but the time-dependent and geography-dependent variability limits their application as power resources [1,2]. Hydrogen, as an ideal energy carrier, offers a solution for energy storage and transportation [3]. Metal hydrides, which can reversibly absorb hydrogen in large quantity under mild conditions, have been attracting world-wide attention as the medium for hydrogen storage.

Metal hydrides are categorized into interstitial (e.g., VH_2 and $LaNi_5H_6$) and non-interstitial hydrides (e.g., MgH_2). Vanadium (V)-based alloy, with body centered cubic (BCC) structure, is noteworthy for its high hydrogen storage density and fast hydrogen sorption kinetics [4,5]. Different V-based alloy systems have been developed, including V-Ti-Cr, V-Ti-Cr-Fe, and so on, which exhibits reversible capacities of ~2.5 wt.% under ambient conditions (e.g., 0–80 °C at 10 MPa H_2) [4]. Furthermore, a big progress has been made in economical approaches to prepare V-based alloys, for example, from low-cost ferrovanadium master alloy or directly from oxides [4]. However, it is still a big distance from the practical application of vanadium-based alloys for hydrogen storage.

The hydrogen absorption process is accompanied by significant volume expansion, particularly in interstitial hydrides. For instance, the volume of $LaNi_5$ alloy can increase by about 20% after full hydrogenation [6], and the lattice of vanadium-based alloy can expand by approximately 40% [7]. Such large volume expansion would lead to the pulverization of alloy particles and reduce the heat and mass transfer efficiency within the

tank [8], unavoidably imposing substantial stress on hydrogen storage tanks, potentially causing deformation or rupture [9,10]. Turning powders into compact after mixing with additives (such as binder and anti-expansion agent) could alleviate the impact of volume expansion of the metal hydrides [11–16]. For example, the LaNi₅ compact, made from 1 mm LaNi₅ powders and resin, shows very stable structure with only a small amount of powder detached after 100 hydrogen sorption cycles [17]. Tarasov [18] et al. employed a graphene–nickel composite to enhance the desorption reaction of magnesium hydride. While the graphene–nickel material facilitated the magnesium hydride desorption reaction, the graphene component was prohibitively expensive for large-scale implementation. Compacts of Mg₉₀Ni₁₀ powder and Ti-Mn-based powder after mixing with expanded graphite (ENG) could increase the thermal conductivity of the metal hydride bed and reduce the stress during the hydrogen sorption process [19]. There are also some studies on the preparation of membranes with hydrogen selective permeability using polymers mixed with metal hydrides [20]. However, few investigations focusing on the volume expanding behaviors of V-based hydrogen storage alloys during hydrogen sorption have been reported.

In the present study, we designed and constructed a dedicated expansion test apparatus to evaluate the in situ volume expansion of V-based alloy, V₆₁Cr₂₄Ti₁₂Ce₃ (at.%), during the hydrogen absorption process. Organic silicone gel, also known as PDMS, is a commercially available highly elastic polymer composed primarily of silicone oil and a curing agent. Its curing process is relatively straightforward, and it has been demonstrated to be non-toxic to V-Ti-Cr-Fe alloys [21]. So, the compact, composed of V₆₁Cr₂₄Ti₁₂Ce₃ powders, organic silica gel (PDMS) [22] and graphite flakes, was designed to reduce the volume expansion.

2. Results and Discussions

The pressure–composition–temperature (PCT) curves of the V₆₁Cr₂₄Ti₁₂Ce₃ alloy for hydrogen absorption (Figure 1a) and desorption (Figure 1b) were measured at 0 °C, 18 °C, and 50 °C, respectively. The hydrogen desorption plateau pressure (P_{eq}) of the V₆₁Cr₂₄Ti₁₂Ce₃ alloy at 18 °C reaches 4.6 bar, which meets with the requirement of entry pressure for the operation of fuel cell. Based on the desorption PCT curves in Figure 1b, the V₆₁Cr₂₄Ti₁₂Ce₃ alloy achieves a reversible hydrogen storage capacity of 2.51 wt.% at 50 °C within the pressure region of 0.01–10 MPa. The van't Hoff plots, obtained by plotting P_{eq} versus 1/T, are shown in Figure 1c. The enthalpy change (ΔH) and entropy change (ΔS) are derived and listed in Table 1.

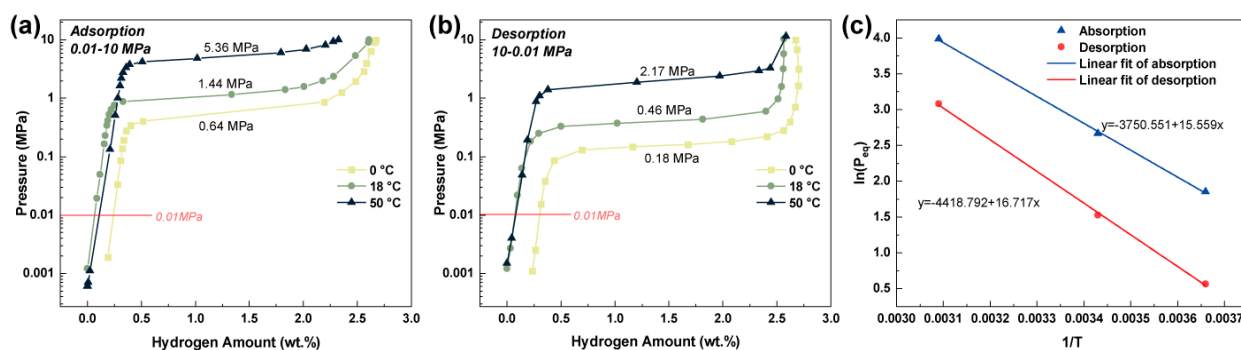


Figure 1. The PCT curves (a,b) and van't Hoff plots (c) of V₆₁Cr₂₄Ti₁₂Ce₃ alloy.

Table 1. The enthalpy change (ΔH) and the entropy change (ΔS) of the V₆₁Cr₂₄Ti₁₂Ce₃ alloy.

Properties	Hydrogen Absorption	Hydrogen Desorption
ΔH (kJ/mol H ₂)	−31.18	36.74
ΔS (J/mol H ₂)	−129.36	138.99

Figure 2a,b show the X-ray diffraction (XRD) patterns of the $V_{61}Cr_{24}Ti_{12}Ce_3$ alloy before and after hydrogenation, respectively. Before hydrogenation, the $V_{61}Cr_{24}Ti_{12}Ce_3$ alloy shows the typical BCC structure, with $a = 0.3031(1)$ Å and $V = 0.02785$ Å³, as presented in Table 2. After hydrogenation, the minor $V_4H_{2.88}$ -type BCT phase and the major VH_2 -type FCC phase are observed, attributed to subsequent phase transition from BCC to BCT and from BCT to FCC during the hydrogen absorption process (Figure 2c). The BCT phase shows the lattice parameters of $a = 0.3143(0)$ Å and $c = 0.3148(3)$ Å, and lattice volume increases up to $V = 0.03110$ Å³, with a lattice expansion ratio of 11.67% compared to the BCC phase. The FCC phase shows the lattice parameters of $a = 0.4250(3)$ Å, and lattice volume increases up to $V = 0.07678$ Å³, with an expansion ratio of 23.44% compared to the BCT phase and an expansion ratio of 37.85% compared to the BCC phase.

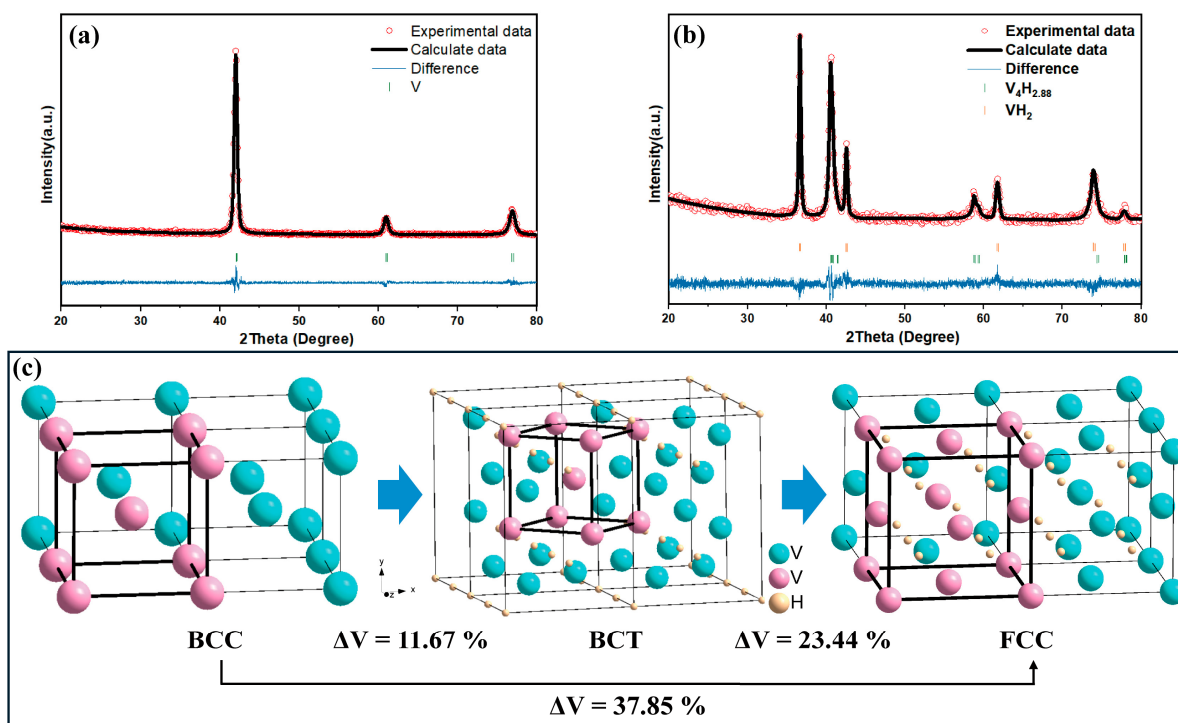


Figure 2. The XRD patterns of the $V_{61}Cr_{24}Ti_{12}Ce_3$ alloy before (a) and after (b) hydrogenation, and the schematic diagram of the $V_{61}Cr_{24}Ti_{12}Ce_3$ alloy volume expansion (c).

Table 2. Lattice constants BCC, BCT, and FCC phases in $V_{61}Cr_{24}Ti_{12}Ce_3$ alloy.

Phase	a (Å)	b (Å)	c (Å)	V (Å ³)
BCC	0.3031(1)	0.3031(1)	0.3031(1)	0.02785
BCT	0.3143(0)	0.3143(0)	0.3148(3)	0.03110
FCC	0.4250(3)	0.4250(3)	0.4250(3)	0.07678

Figure 3a,b show the hydrogen absorption plots of the pure powder bed and the compact bed with a diameter of 10 mm after five cycles. Both beds contain the same amount of alloy for testing. The first absorption reaction was conducted at 0 °C, and the rest of the absorption reactions were carried out at 20 °C. The powder bed shows the fast absorption kinetics at the first absorption cycle (Figure 3a), which reached saturation within 10 min with the absorption capacity of 3.5 wt.%. In the following four cycles, the powder bed could absorb hydrogen at ~2.0 wt.% within 10 min. In contrast, the compact bed shows slightly slower absorption kinetics at the first absorption cycle, which requires approximately 20 min to reach the saturation state with a capacity of 3.4 wt.%. In the subsequent four cycles, the powder bed displays much faster absorption kinetics with a

hydrogen absorption amount of ~2.0 wt.% within 5 min. Furthermore, the compact bed still maintains its structure after five cycles, as shown in Figure 3c,d.

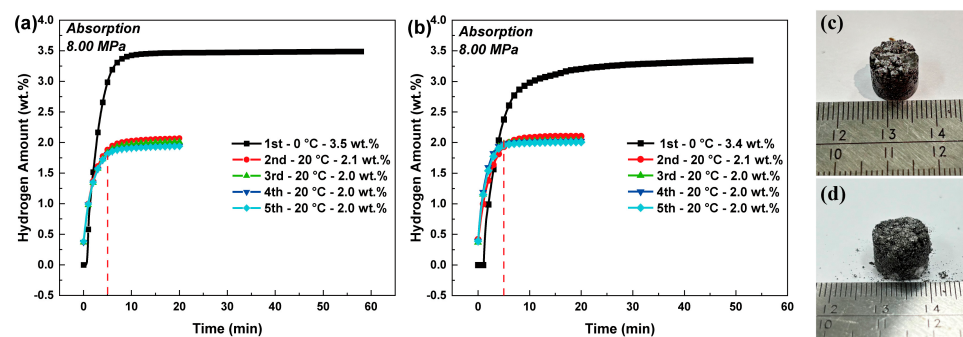


Figure 3. The hydrogen absorption plots of (a) the pure powder bed and (b) the compact bed within 5 cycles; the images of compact bed: (c) initial state and (d) after 5 cycles.

Figure 4a presents real-time data of position sensor for the $V_{61}Cr_{24}Ti_{12}Ce_3$ alloy powder bed during the five cycles of hydrogen absorption and desorption, which was measured using the self-made in situ expansion testing device shown in Figure 7. The time required for the powder bed to complete the hydrogen sorption reaction is 72, 49, 54, 58, and 59 min, for the first to fifth cycles, respectively. The powder bed was vibrated after the completion of each hydrogen absorption and desorption cycle. The volume expansion ratio in each cycle was calculated by comparing the height after hydrogen absorption of the current cycle with the height after hydrogen desorption in the initial cycle, as shown in Figure 4b. The alloy powder shows the highest expansion ratio of 131% at the first hydrogen absorption cycle, assigned to the phase evolution from BCC to FCC of $V_{61}Cr_{24}Ti_{12}Ce_3$. The expansion ratio decreases to 45% in the second cycle and stabilizes between 40% and 43% from the third to the fifth cycle. Figure 4c presents the particle size distribution of alloy powder after five hydrogen absorption/desorption cycles. The size of the majority of the powder decreases to below 0.355 mm, much smaller than the initial particle size of 3.35 mm.

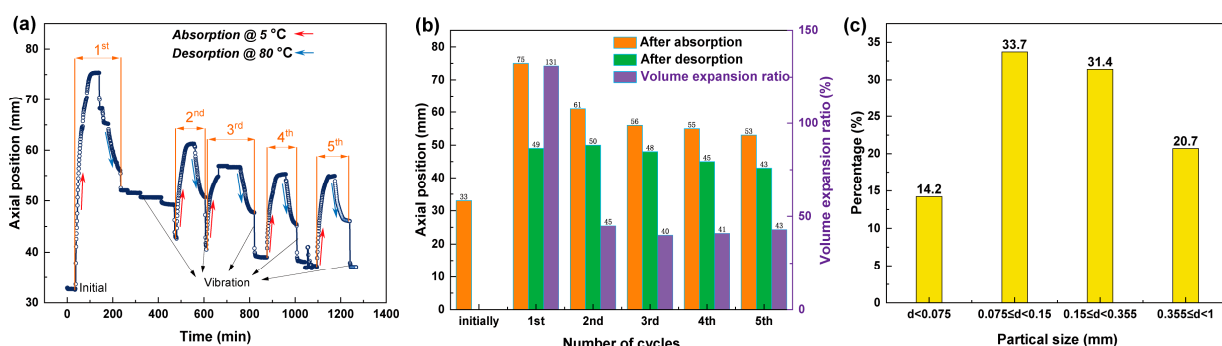


Figure 4. The height change (a) and volume expansion ratio (b) of the $V_{61}Cr_{24}Ti_{12}Ce_3$ alloy powder bed during the 5 cycles. The particle size (c) of $V_{61}Cr_{24}Ti_{12}Ce_3$ alloy powder after 5 cycles.

Figure 5a presents real-time data from the position sensor for compact bed during the five cycles. The compact bed was vibrated after the completion of each hydrogen absorption and desorption cycle. Figure 5b shows the corresponding positional information of the position sensor and the volume expansion ratio of each cycle. The expansion ratio of the first hydrogen absorption cycle is calculated to be 97%, a reduction of 34% compared to the alloy powder bed. The volume expansion ratio of the second cycle decreases to 21% and stabilizes at 13% afterwards. Additionally, the durations required for the compact bed to complete the hydrogen sorption reaction are 91, 39, 44, 41, and 33 min for the first to the fifth cycle, respectively, which are significantly shortened compared to the values for the alloy powder bed in Figure 4a. Hence, the conversion of powder bed to

compact bed accelerates the hydrogen absorption kinetics, probably attributed to improved effective thermal conductivity. Figure 5c,d show the initial state of the compact bed before and after five hydrogen sorption cycles, respectively. The shape of the compact bed was basically maintained.

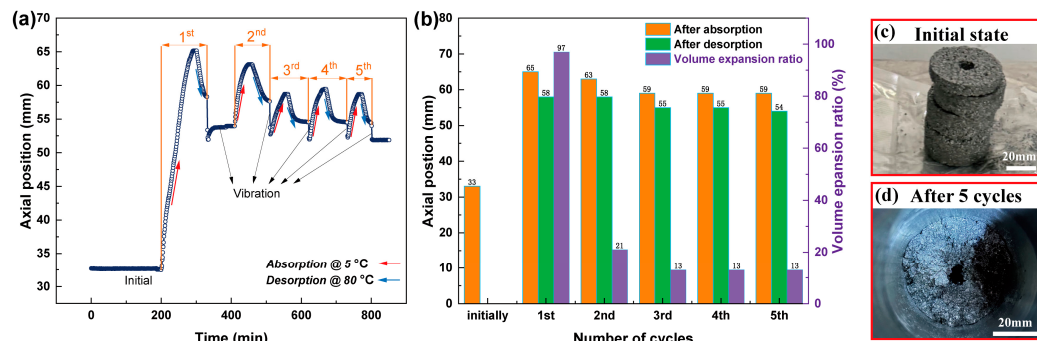


Figure 5. The height change (a) and volume expansion rate (b) of the compaction of $V_{61}Cr_{24}Ti_{12}Ce_3$ alloy powder during the 5 cycles. The state of composite hydrogen storage material before hydrogen absorption (c) and after 5 cycles (d).

For the two beds, the largest volume expansion was observed at the first cycle, which is attributed to lattice expansion during the phase transition of the $V_{61}Cr_{24}Ti_{12}Ce_3$ alloy from BCC to FCC structure. Since the second cycle, the volume expansion ratio of the powder bed almost stabilizes at 40–45%, accompanied with the phase transition from BCT to FCC. The compact bed shows a much smaller volume expansion ratio of 21% at the second cycle, which further decreases and stabilizes at 13% after the third cycle. The slight decrease in volume expansion ratio from the second to the third cycle may be attributed to continuous pulverization of $V_{61}Cr_{24}Ti_{12}Ce_3$ alloy powder or slow formation process of the stable silicone elastomers.

Note that after the completion of each cycle, the powder bed and compact bed were vibrated. The sensor positions after vibration are listed in Table 3. For the powder bed, sensor position after vibration decreases continuously from the first to the fifth cycle, implying that the bed became more compact after vibration probably owing to the pulverization of alloy powders. Differently, the sensor position of the compact bed changes slightly and keeps almost constant from the third to the fifth cycle, indicative of the formation of stable bed.

Table 3. The sensor position after vibration for each circle.

Sensor Movement Distance Caused by Vibration (mm)	1st	2nd	3rd	4th	5th
Powder bed	42.88	40.54	38.99	37.10	36.00
Compact bed	53.95	52.73	51.99	52.27	51.86

SEM and EDS analyses were conducted on the compact bed after five cycles, as illustrated in Figure 6. SEM and mapping results in Figure 6(a,a1,a2) reveal that graphite flakes and organosilicon gel are uniformly distributed on the surface of the alloy particles. Figure 6b-d demonstrate that the organic silica gel (PDMS) effectively binds the pulverized particles. Graphite has a lubricating effect, which could reduce the friction between particles [23]. Organic silica gel (PDMS) cured like ethylene-vinyl acetate copolymer is highly elastomeric, which not only secures the graphite flakes tightly to the alloy particles but also fixes the alloy particles in situ. Accordingly, the utilization of a combination of alloy particles, organic silica gel (PDMS), and graphite flakes in the form of a compact bed not only effectively mitigates the volume expansion of the alloy bed but also contributes to the immobilization of the pulverized alloy powders.

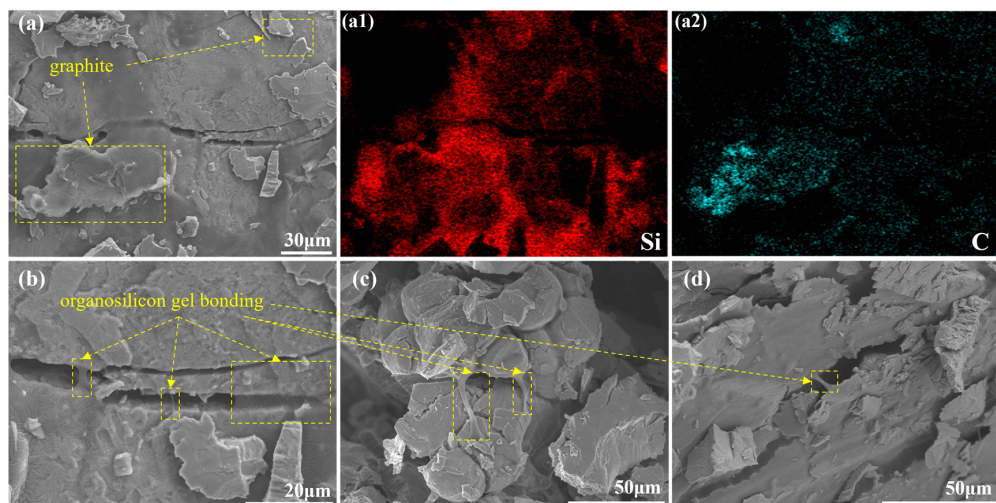


Figure 6. (a–d) The SEM images of the compact bed after 5 cycles and elemental mapping (a1,a2) of Si and C corresponding to figure (a).

3. Materials and Methods

The $V_{61}Cr_{24}Ti_{12}Ce_3$ alloy was prepared via floating melting with raw materials of V (purity: 99.9%), Ti (purity: 99.6%), Cr (purity: 99.6%) and Fe (purity: 99.9%). The as-cast $V_{61}Cr_{24}Ti_{12}Ce_3$ alloy was annealed at 1400 °C for 0.5 h under dynamic vacuum. The as-annealed alloy was crushed to a powder size of ~3.35 mm using a jaw crusher under nitrogen atmosphere.

The alloy powders were mixed with graphite flake (Macklin Biochemical Technology Co., Ltd., Shanghai, China) and organosilicon gel (Sylgard 184, Dow Corning, Midland, MI, America) with a mass ratio of 92%: 4%: 4%. The mixture was subjected to a pressing and molding process, with a pressure of 500 MPa maintained for a duration of one minute. Two types of compact bed, one with a diameter of 10 mm and another with an inner diameter of 10 mm and an outer diameter of 45 mm, were prepared. Prior to the commencement of cycling tests, the compact bed was stored at room temperature for ≥ 24 h in an Ar-circulated glove box to allow the silicone gel to fully cure and form an elastomer.

Alloy powders were loaded in a stainless-steel reactor for pressure–composition–temperature (PCT) measurement. To activate the alloy for hydrogen sorption, the alloy powders were evacuated for 1 h at room temperature, followed by the introduction of hydrogen at 7.5 MPa. The alloy powders could fast react with hydrogen at room temperature. The hydrogen absorption PCT curves were measured at 0, 18, and 50 °C. To measure the hydrogen desorption PCT curves, the alloy powders were fully hydrogenated at 0 °C under 7.5 MPa H₂, and subsequently, the temperature of the reactor was set to the targeting temperatures of 0, 18, and 50 °C, respectively. The measurement of hydrogen desorption PCT measurement started after the hydrogen pressure became stable. The X-ray diffraction (XRD) measurements were conducted using Cu K α radiation (Rigaku, Tokyo, Japan), and the XRD data were analyzed using FullProf 2023 [24]. Microstructures was observed via scanning electron microscope (SEM, JSM-7800F, JEOL Ltd., Tokyo, Japan).

To investigate the actual expansion of the $V_{61}Cr_{24}Ti_{12}Ce_3$ alloy during the hydrogen absorption process, an in situ expansion testing device was designed and a corresponding testing platform was established, as depicted in Figure 7. The testing device contains the expansion test reactor, two water baths, and a flow and pressure controller. A steel plate together with a position sensor was placed on top of the sample. The sensor could measure the position of the steel plate, which reflects the volume change in the tested sample. Two water baths were maintained to offer cold and hot water for the hydrogen absorption and desorption processes, respectively. The hydrogen flows and pressures during the testing process could be controlled and monitored from the test platform which was equipped with flow meters and pressure sensors. Before testing, the alloy powder bed or compact

bed was activated under vacuum for 2 h, followed by the introduction of 7.5 MPa H₂ at 5 °C. The hydrogen desorption was carried out under a dynamic vacuum at 80 °C. The hydrogen absorption and desorption cycle were repeated 5 times.

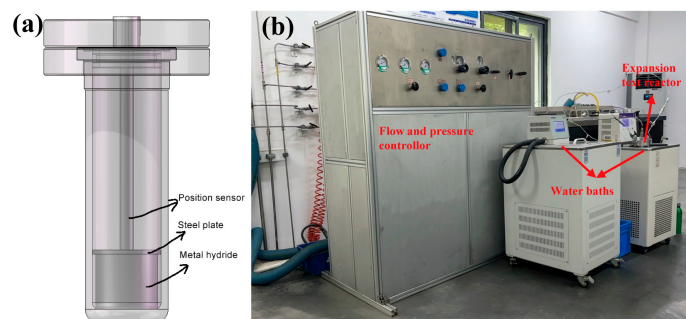


Figure 7. The schematic image of in situ expansion testing tank (a) and the test platform (b).

4. Conclusions

We have demonstrated the volume expansion behavior of the V₆₁Cr₂₄Ti₁₂Ce₃ alloy measured using the self-made volume expansion test device. Firstly, the maximum reversible capacity of V₆₁Cr₂₄Ti₁₂Ce₃ alloy is 2.51 wt.%, and the lattice expansion of V₆₁Cr₂₄Ti₁₂Ce₃ alloy in the saturated state of hydrogen absorption is found to be 37.85% and is analyzed via XRD test. The powder bed of the V₆₁Cr₂₄Ti₁₂Ce₃ alloy shows a large volume expansion ratio of 131% at the first hydrogen absorption cycle and 40~45% in the following four cycles. The compact bed, made of alloy powders, organic silicone gel (PDMS), and graphite flakes, shows a significantly smaller volume expansion ratio, which is 97% at the first cycle and 21% at the second cycle, and stabilizes at 13% in the following cycles. The highly elastic organic silicone gel (PDMS) serves to retain the graphite flakes on the alloy particles. Furthermore, the lubrication of the graphite flakes serves to reduce the interaction force between the powder particles. So, the addition of organic silicone gel and graphite flakes contributes to the formation of a stable bed of V₆₁Cr₂₄Ti₁₂Ce₃ alloy, which does not reduce the hydrogen absorption capacity but improves the hydrogen absorption kinetics after the second cycle.

Author Contributions: Data curation, Q.H. and H.K.; testing, Y.H. and Y.C.; writing—original draft preparation, M.L.; editing, Y.Y. All authors have read and agreed to the published version of the manuscript.

Funding: This study was financially supported by Sichuan Science and Technology Program (No. PG-PGFT-JFKF23-000009-0) and Xizang Autonomous Region Key R&D Program (XZ202401ZY0096).

Data Availability Statement: All data generated or analyzed during this study are included in this article.

Conflicts of Interest: The authors declare no conflicts of interest.

References

- Chen, Z.; Ma, Z.; Zheng, J.; Li, X.; Akiba, E.; Li, H.W. Perspectives and challenges of hydrogen storage in solid-state hydrides. *Chin. J. Chem. Eng.* **2021**, *29*, 1–12. [[CrossRef](#)]
- Dieterich, M.; Pohlmann, C.; Bürger, I.; Linder, M.; Röntzsch, L. Long-term cycle stability of metal hydride-graphite composites. *Int. J. Hydrogen Energy* **2015**, *40*, 16375–16382. [[CrossRef](#)]
- Schlüpbach, L.; Züttel, A. Hydrogen-storage materials for mobile applications. *Nature* **2001**, *414*, 353–358. [[CrossRef](#)]
- Kong, H.Y.; Xie, Q.F.; Wu, C.L.; Wang, Y.; Chen, Y.G.; Li, H.W.; Yan, Y.G. Vanadium-based alloy for hydrogen storage: A review. *Rare Met.* **2024**, *6201–6232*. [[CrossRef](#)]
- Matsushita, M.; Monde, M.; Mitsutake, Y. Experimental formula for estimating porosity in a metal hydride packed bed. *Int. J. Hydrogen Energy* **2013**, *38*, 7056–7064. [[CrossRef](#)]
- Cuscueta, D.J.; Silin, N.; Melnichuk, M. Stress reduction in a hydride container by the addition of a glidant agent. *Int. J. Hydrogen Energy* **2020**, *45*, 27452–27456. [[CrossRef](#)]

7. Luo, L.; Wu, C.; Yang, S.; Zhou, J.; Chen, Y.; Yang, F.; Xu, Y.; Liu, P. Decaying behaviors of V₄₀(TiCr)₅₁Fe₈Mn hydrogen storage alloys with different particle sizes. *J. Alloys Compd.* **2015**, *645*, S178–S183. [[CrossRef](#)]
8. Herbrig, K.; Pohlmann, C.; Gondek, Ł.; Figiel, H.; Kardjilov, N.; Hilger, A.; Manke, I.; Banhart, J.; Kieback, B.; Röntzsich, L. Investigations of the structural stability of metal hydride composites by in-situ neutron imaging. *J. Power Sources* **2015**, *293*, 109–118. [[CrossRef](#)]
9. Wu, Z.; Yang, C.; Yan, Y.; Wang, Y.; Tang, X.; Chen, Y.; Li, J.; Wang, M.; Xie, Q.; Chen, Y.; et al. Effect of dehydrogenation depth on cyclic hydrogen desorption properties of V₄₀Ti_{25.5}Cr_{26.5}Fe₈ alloy. *J. Alloys Compd.* **2023**, *955*, 170036. [[CrossRef](#)]
10. Heubner, F.; Pohlmann, C.; Mauermann, S.; Kieback, B.; Röntzsich, L. Mechanical stresses originating from metal hydride composites during cyclic hydrogenation. *Int. J. Hydrogen Energy* **2015**, *40*, 10123–10130. [[CrossRef](#)]
11. Charlas, B.; Gillia, O.; Doremus, P.; Imbault, D. Experimental investigation of the swelling/shrinkage of a hydride bed in a cell during hydrogen absorption/desorption cycles. *Int. J. Hydrogen Energy* **2012**, *37*, 16031–16041. [[CrossRef](#)]
12. Wu, K.; Cai, B.; Fan, L.; Qin, L.; Chen, D.; Huang, Y. Stress measurement of MnNi_{4.5}Cr_{0.45}Mn_{0.05} alloy during hydrogen absorption-desorption process in a cylindrical reactor. *Int. J. Hydrogen Energy* **2020**, *45*, 28175–28182. [[CrossRef](#)]
13. Gattia, D.M.; Jangir, M.; Jain, I.P. Behavior of Compacted Magnesium-Based Powders for Energy-Storage Applications. *Inorganics* **2020**, *8*, 54. [[CrossRef](#)]
14. Duan, W.; Du, J.; Wang, Z.; Niu, Y.; Huang, T.; Li, Z.; Pu, C.; Wu, Z. Strain variation on the reaction tank of high hydrogen content during hydrogen absorption/desorption cycles. *Int. J. Hydrogen Energy* **2013**, *38*, 2347–2351. [[CrossRef](#)]
15. Gabriel, R.A.N.; Cesar, A.G.B.; Daniel, R.L.; Luiz, A.P. Polyetherimide-LaNi₅ composite films for hydrogen storage applications. *Int. J. Hydrogen Energy* **2021**, *46*, 32767–32778. [[CrossRef](#)]
16. Shiraz, H.G.; Tavakoli, O. Investigation of graphene-based systems for hydrogen storage. *Renew. Sustain. Energy Rev.* **2017**, *74*, 104–109. [[CrossRef](#)]
17. Kazuya, K.; Yoshinori, K.; Hideaki, I. Development of large MH tank system for renewable energy storage. *Int. J. Hydrogen Energy* **2017**, *42*, 22475–22479. [[CrossRef](#)]
18. Tarasov, B.P.; Arbuzov, A.A.; Mozhzhuhin, S.A.; Volodin, A.A.; Fursikov, P.V. Composite materials with 2D graphene structures: Applications for hydrogen energetics and catalysis with hydrogen participation. *J. Struct. Chem.* **2018**, *59*, 830–838. [[CrossRef](#)]
19. Carsten, P.; Lars, R.; Siarhei, K.; Thomas, H.; Bernd, K. Magnesium alloy-graphite composites with tailored heat conduction properties for hydrogen storage applications. *Int. J. Hydrogen Energy* **2010**, *35*, 12829–12836. [[CrossRef](#)]
20. Strugova, D.V.; Zadorozhnyy, M.Y.; Berdonosova, E.A.; Yablokova, M.Y.; Konik, P.A.; Zheleznyi, M.V.; Semenov, D.V.; Milovzorov, G.S.; Padaki, M.; Kaloshkin, S.D.; et al. Novel process for preparation of metal-polymer composite membranes for hydrogen separation. *Int. J. Hydrogen Energy* **2018**, *43*, 12146–12152. [[CrossRef](#)]
21. Zheng, X.; Kong, H.Y.; Chu, D.S.; Hu, F.P.; Wang, Y.; Yan, Y.G.; Wu, C.L. Stress Reduction of a V-Based BCC Metal Hydride Bed Using Silicone Oil as a Glidant. *Inorganics* **2022**, *10*, 167. [[CrossRef](#)]
22. Marc, P.W.; Georgette, B.; Salieb, B.; Patrick, H. PDMS with designer functionalities-properties, modifications strategies, and applications. *Prog. Polym. Sci.* **2018**, *83*, 97–134. [[CrossRef](#)]
23. Warfsmann, J.; Puszkiel, J.A.; Passing, M.; Krause, P.S.; Wienken, E.; Taube, K.; Klassen, T.; Pistidda, C.; Jepsen, J. Applying wash coating techniques for swelling-induced stress reduction and thermal improvement in metal hydrides. *J. Alloys Compd.* **2023**, *950*, 169814. [[CrossRef](#)]
24. Rodríguez-Carvajal, J. Recent advances in magnetic structure determination by neutron powder diffraction. *Phys. B Condens. Matter* **1993**, *192*, 55–69. [[CrossRef](#)]

Disclaimer/Publisher’s Note: The statements, opinions and data contained in all publications are solely those of the individual author(s) and contributor(s) and not of MDPI and/or the editor(s). MDPI and/or the editor(s) disclaim responsibility for any injury to people or property resulting from any ideas, methods, instructions or products referred to in the content.